Modelling precipitation sequences in power plant steels Part 1 – Kinetic theory

J. D. Robson and H. K. D. H. Bhadeshia

The ability of steels to resist creep deformation depends on the presence in the microstructure of carbides and intermetallic compounds which precipitate during tempering or during elevated temperature service. The precipitation occurs in a sequence which leads towards thermodynamic equilibrium. The present paper deals with an extension of the Johnson–Mehl–Avrami theory for overall transformation kinetics. The modification permits the treatment of more than one precipitation reaction occurring simultaneously, a feature which is found to be essential for representing the reactions observed experimentally in a wide range of secondary hardening steels. *MST/3604*

 Manuscript received 25 April 1996. *The authors are in the Department of Materials Science and Metallurgy, University of Cambridge, Pembroke Street, Cambridge, UK.*

Introduction

Steels used in the manufacture of power plant range from those designed to resist creep deformation at temperatures ~600°C to others which are exposed to relatively low temperatures where the primary design criterion is toughness.[1,2] The microstructures of power plant alloys often consist of δ ferrite, martensite, bainite, allotriomorphic ferrite, and retained austenite as the major phases obtained following a normalising heat treatment. However, these microstructures are then subjected to very severe tempering (~700°C for several hours) causing general coarsening and the precipitation of ever more stable alloy carbides and intermetallic compounds. It is these solid state reactions which ultimately determine the mechanical stability of the steels and, hence, their useful design lives.

The purpose of the present work was to model the kinetics of carbide and Laves phase precipitation reactions that occur in power plant steels over long periods of time at elevated temperatures: in other words, to produce time–temperature–transformation diagrams for tempering reactions as a function of steel chemical composition and tempering temperature. It has been necessary, therefore, to develop theory capable of handling several simultaneous precipitation reactions whereby the different phases influence each other, for example by drawing the same solute from the matrix ferrite.

Overall transformation kinetics

The evolution of volume fraction during solid state transformation can be modelled using the classical Johnson–Mehl–Avrami theory, which has been reviewed by Christian.[3] It is necessary briefly to introduce this theory to set the scene for the modifications made to allow for simultaneous reactions.

A given precipitate particle effectively forms after an incubation period τ. Assuming growth at a constant rate g, the volume w_τ of a spherical particle is given by

$$w_\tau = (4\pi/3)g^3(t-\tau)^3 \, d\tau \quad t > \tau \quad . \quad . \quad . \quad . \quad . \quad . \quad . \quad . \quad . \quad (1)$$

$$w_\tau = 0 \quad t < \tau \quad . \quad . \quad . \quad . \quad . \quad . \quad . \quad . \quad . \quad . \quad . \quad . \quad . \quad (2)$$

where t is the time defined to be zero at the instant the sample reaches the isothermal transformation temperature.

Particles nucleated at different locations may eventually touch; this problem of hard impingement is neglected at first, by allowing particles to grow through each other and by permitting nucleation to happen even in regions which have already transformed. The calculated volume of β phase is therefore an extended volume; the change in extended volume dV_β^e is given by

$$dV_\beta^e = w_\tau I V \, d\tau \quad . \quad . \quad . \quad . \quad . \quad . \quad . \quad . \quad . \quad . \quad . \quad . \quad . \quad (3)$$

i.e.

$$V_\beta^e = (4\pi V/3) \int_{\tau=0}^{t} g^3 I (t-\tau)^3 \, d\tau \quad . \quad . \quad . \quad . \quad . \quad . \quad . \quad . \quad (4)$$

where V is the total sample volume and I is the nucleation rate. Notice that it is possible to follow the evolution of each extended particle individually.

Only those parts of the change in extended volume which lie in untransformed regions of the parent phase can contribute to the change in real volume of β. The probability that any change in extended volume lies in untransformed parent material is proportional to the fraction of untransformed material. It follows that the actual change in volume

$$dV_\beta = \left(1 - \frac{V_\beta}{V}\right) dV_\beta^e \quad . \quad . \quad . \quad . \quad . \quad . \quad . \quad . \quad . \quad . \quad . \quad . \quad (5)$$

$$V_\beta^e = -V \ln\left(1 - \frac{V_\beta}{V}\right) \quad (6)$$

so th

$$-\ln\left(1 - \frac{V_\beta}{V}\right) = (4\pi/3)g^3 \int_0^t I(t-\tau)^3 \, d\tau \quad . \quad . \quad . \quad . \quad (7)$$

In making this conversion from extended to actual volume, all information about individual particles is lost, so that the application of the Avrami model can only yield average quantities such as grain size and volume fraction, but not grain size distribution or grain volume distribution.

The approach described above is limited to the precipitation of a single phase. The theory can be applied to cases where more than one decomposition reaction occurs if the individual reactions occur over different temperature ranges, i.e. they occur successively and largely independently.[4–6] However, a great deal of fruitless work demonstrated that the evolution of carbides during the tempering of steels can not be treated in this way. Precipitation and dissolution reactions during tempering overlap significantly, with profound interactions between the different precipitates. Consequently, the Johnson–Mehl–Avrami approach has been adapted to deal with many reactions occurring simultaneously.

Simultaneous reactions

The principles involved are first illustrated by a simplified example in which β and θ precipitate at the same time

from the parent phase which is designated α. It is assumed that the nucleation and growth rates do not change with time and that the particles grow isotropically.

The increase in the extended volume owing to particles nucleated in a time interval $t=\tau$ to $t=\tau+\mathrm{d}\tau$ is, therefore, given by

$$\mathrm{d}V_\beta^e = 4/3\pi g_\beta^3 (t-\tau)^3 I_\beta(V)\,\mathrm{d}\tau \quad \ldots\ldots\ldots (8)$$

$$\mathrm{d}V_\theta^e = 4/3\pi g_\theta^3 (t-\tau)^3 I_\theta(V)\,\mathrm{d}\tau \quad \ldots\ldots\ldots (9)$$

where g_β, g_θ, I_β, and I_θ are the growth and nucleation rates of β and θ respectively, all of which are assumed here to be independent of time, and V is the total volume of the system. For each phase, the increase in extended volume will consist of three separate parts. These are, for β:

(i) β which has formed in untransformed α
(ii) β which has formed in regions which are already β
(iii) β which has formed in regions which are already θ.

Only β formed in untransformed α will contribute to the real volume of β. On average, a fraction $[1-(V_\beta+V_\theta)/V]$ of the extended volume will be in previously untransformed material. It follows that the increase in real volume of β is given by

$$\mathrm{d}V_\beta = \left(1-\frac{V_\beta+V_\theta}{V}\right)\mathrm{d}V_\beta^e \quad (10)$$

nd, similarly for θ

$$\mathrm{d}V_\theta = \left(1-\frac{V_\beta+V_\theta}{V}\right)\mathrm{d}V_\theta^e \quad \ldots\ldots\ldots (11)$$

Generally, V_β will be some complicated function of V_θ and it is not possible to integrate these expressions to find the relationship between the actual and extended volumes. However, in certain simple cases, it is possible to relate V_β to V_θ by multiplication with a suitable constant K. It is then possible to write

$$V_\theta = KV_\beta \quad \ldots\ldots\ldots (12)$$

The equations relating the increment in the actual volume to that of the extended volume may now be written as

$$\mathrm{d}V_\beta = \left(1-\frac{V_\beta+KV_\beta}{V}\right)\mathrm{d}V_\beta^e \quad \ldots\ldots\ldots (13)$$

$$\mathrm{d}V_\theta = \left(1-\frac{V_\theta+KV_\theta}{KV}\right)\mathrm{d}V_\theta^e \quad \ldots\ldots\ldots (14)$$

Equations (13) and (14) may then be integrated to find an analytical solution relating the extended and actual volumes analogous to that for single phase precipitation

$$\frac{V_\beta^e}{V} = \frac{-1}{1+K}\ln\left[1-\frac{V_\beta}{V}(1+K)\right] \quad \ldots\ldots\ldots (15)$$

$$\frac{V_\theta^e}{V} = \frac{-K}{1+K}\ln\left[1-\frac{V_\theta}{V}\left(\frac{1+K}{K}\right)\right] \quad \ldots\ldots\ldots (16)$$

The total extended volume is found for each phase by integrating equations (8) and (9) with respect to τ. After rearranging, the final expressions for the volume fractions ζ of β and θ phases are

$$\zeta_\beta = \left(\frac{1}{1+K}\right)\left\{1-\exp\left[-\frac{1}{3}(1+K)\pi g_\beta^3 I_\beta t^4\right]\right\} \quad (17)$$

$$\zeta_\theta = \left(\frac{K}{1+K}\right)\left\{1-\exp\left[-\frac{1}{3}\left(\frac{1+K}{K}\right)\pi g_\theta^3 I_\theta t^4\right]\right\} \quad (18)$$

These equations resemble the well known Avrami equation for single phase precipitation with extra factors to account for the presence of a second precipitate phase. When the volume fraction of both precipitating phases is very small, equations (17) and (18) approximate to the expressions for each phase precipitating alone. This is because in the early stages of transformation, nearly all of the extended volume lies in previously untransformed material and contributes to the actual volume. As transformation proceeds, the volume fraction of each phase predicted for the phases precipitating simultaneously becomes less than that predicted if the phases were precipitating alone. This is what is expected, since additional phases reduce the fraction of the extended volume which lies in previously untransformed material.

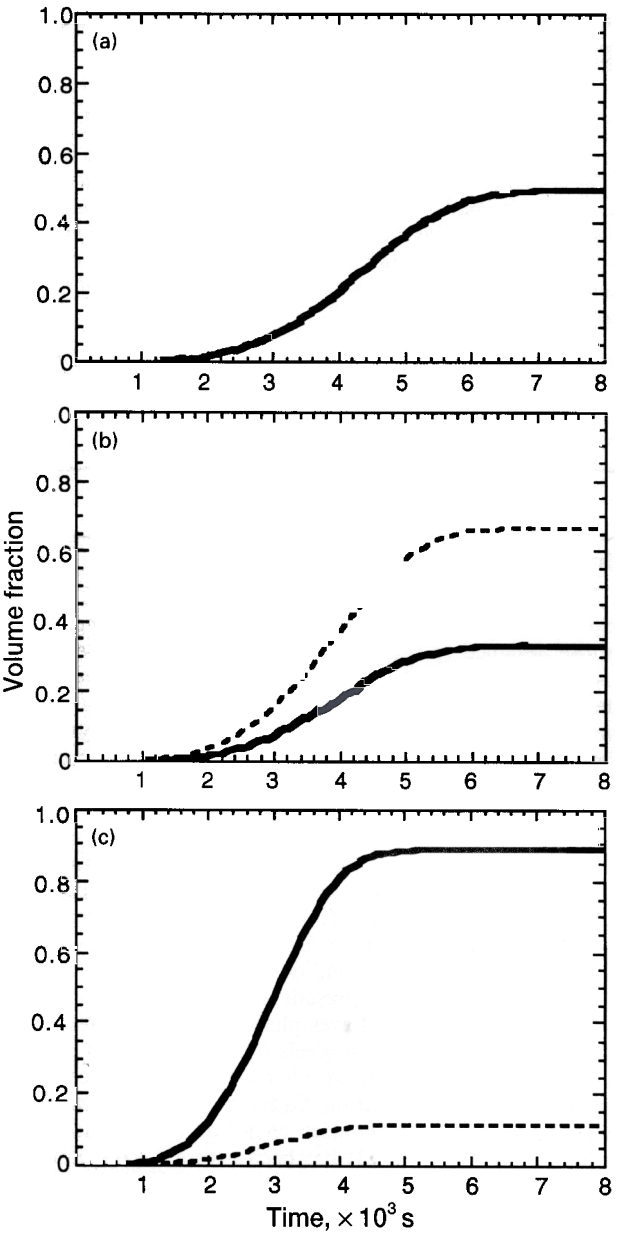

—— β; - - - - θ
a two phases have identical nucleation and growth rates; *b* identical growth rates but θ has twice nucleation rate of β; *c* identical nucleation rates but θ particles growing at twice rate of β particles

1 Simultaneous precipitation of θ and β at given nucleation and growth rates

As the nucleation and growth rates were assumed to be constant, it is possible explicitly to calculate the value of K. The volume of each phase at any time depends on its nucleation rate and the cube of its growth rate. The ratio V_θ/V_β is then constant and given by

$$K = \frac{V_\theta}{V_\beta} = \frac{I_\theta g_\theta^3}{I_\beta g_\beta^3} \quad (19)$$

Some examples of calculations for the case of linear (i.e. constant) growth are shown in Fig. 1. When the nucleation and growth rates of β and θ are set to be identical, their curves for volume fraction v. time are exactly superimposed and each phase eventually achieves a fraction of 0·5 (Fig. 1*a*). When the nucleation rate of θ is set to be twice that of β, then, for identical growth rates, the terminal fraction of θ is, as expected, twice that of β (Fig. 1*b*). The case where the growth rate of θ is set to be twice that of β but with identical nucleation rates is illustrated in Fig. 1*c*. The final volume fraction of the θ phase is eight times that of the β phase because volume fraction is a function of the growth rate cubed.

Complex simultaneous reactions

In practice, the multiple reactions found in power plant steels have important complications not included in the simple model described above. The phases interfere with each other, not only by reducing the volume available for transformation, but also by removing solute from the matrix and, thereby, changing its composition. The change in matrix composition changes the growth and nucleation rates of the phases. Therefore, there are no simple constants linking the volume fraction of all the phases and a different approach is needed.

The phases which might precipitate include M_3C, MX, M_2X, M_7C_3, $M_{23}C_6$, M_6C, and Laves phase. It is possible, in principle, to incorporate all these phases into a unified model. However, primary interest was in the 10CrMoV steel in which the predominant phases are those given in Table 1 along with a summary of the nucleation and growth characteristics. In the following discussion, the parent phase (ferrite in this instance) is identified as α and the product phase as β.

The model developed is applicable to a wide range of power plant steels. In the present work, it is applied to precipitation in a newly developed 10CrMoV steel as well as a more traditional 2·25Cr1Mo steel. The compositions of these steels are given in Table 2.

MODEL FOR M_3C ENRICHMENT

There is good evidence that the cementite which forms during the tempering of martensite, or as a consequence of the bainite reaction, grows by a displacive mechanism.[7–10] Such a mechanism must naturally involve the diffusion of carbon, but not of substitutional solutes or iron atoms. The iron/substitutional solute ratio, thus, remains constant everywhere and, subject to that constraint, the carbon achieves equality of chemical potential; the cementite is then said to grow by paraequilibrium transformation.[11–13]

As a consequence of this mechanism of growth, M_3C is far from its equilibrium composition when it first forms. Tempering, therefore, leads to large changes in chemical composition with time as the substitutional solute atoms partition between cementite and ferrite in a direction consistent with equilibrium. The calculated paraequilibrium and equilibrium compositions of cementite in a 10CrMoV steel are given in Table 3.

The results in Table 3 are typical for chromium containing steels; the principal change in going from paraequilibrium to equilibrium involves enrichment in chromium and a complementary rejection of iron into the ferrite. The rate of enrichment is approximately given by[8]

$$c = \bar{c} + \frac{4D^{1/2}(\bar{c} + c^{\alpha\beta})t^{1/2}}{z\pi^{1/2}} \qquad (20)$$

where c represents the concentration of the diffusing species, t is the time since M_3C formation, z is the thickness of the cementite plate, D is the diffusion coefficient for solute in the matrix (it is assumed that the corresponding diffusivity in cementite is identical to that in ferrite), $c^{\alpha\beta}$ is the concentration of the substitutional solute in the ferrite which is in equilibrium with the cementite, and $\bar{c}$ is the mean concentration of the substitutional solute in the alloy. This equation is valid only in the absence of soft impingement (i.e. the overlap of the diffusion fields of adjacent particles). An approximation for soft impingement is presented in the 'Solute partitioning effects' section below. The value for $c^{\alpha\beta}$ was calculated using MTDATA.[14] The diffusion coefficient for chromium in ferrite is given by[15]

$$D = 1{\cdot}5 \times 10^{-4} \exp\left(\frac{-240\,000}{RT}\right) \text{m}^2\,\text{s}^{-1} \qquad (21)$$

where $R = 8{\cdot}314\,32\ \text{J mol}^{-1}\,\text{K}^{-1}$ is the universal gas constant and T is the absolute temperature. The thickness of the cementite plates is unknown, so an estimated value of 1 μm was used based on microstructural observations.[16] The volume fraction V_β of M_3C was estimated using the lever rule and the approximation that any carbon dissolved in the ferrite can be neglected[17]

$$V_\beta = \frac{\bar{c}_C}{c_C^{\beta\alpha}} \qquad (22)$$

where $\bar{c}_C$ is the mean carbon concentration in the alloy and $c_C^{\beta\alpha}$ is the carbon concentration in the cementite ~0·25 atom fraction. The rate at which M_3C will draw chromium from the ferrite will depend on both the rate at which c increases according to equation (20) and the volume fraction of the cementite. This rate is important when considering the effect that cementite enrichment will have on the precipitation of other phases and is discussed further in the 'Solute partitioning effects' section below.

It is easy to show that the enrichment of cementite must be taken into account when considering power plant steels. The calculations illustrated by Fig. 2 are for the classic 2·25Cr1Mo steel studied by Baker and Nutting.[18] When tempered at elevated temperatures, beginning with a martensitic or bainitic microstructure, the following (simplified) sequence of carbide precipitation reactions occurs

$$M_3C \rightarrow M_3C + M_2C \rightarrow M_{23}C_6$$

The cementite that precipitates first is not of the equilibrium composition; it contains far less chromium than is expected from the phase diagram. Figure 2 shows that M_2C would not form at all for temperatures above ~800°C in the presence of equilibrium cementite and, at lower temperatures, the driving force for its formation would be considerably reduced.

Table 1 Phases incorporated in model along with type of growth and nucleation in each case

Phase	Nucleation and growth model
M_3C	No nucleation, but paraequilibrium growth of number of particles followed by change in chemical composition
M_2X	Finite nucleation rate, diffusion controlled linear growth of needles
$M_{23}C_6$	Finite nucleation rate, diffusion controlled parabolic growth of spheroids
Laves phase	Finite nucleation rate, diffusion controlled parabolic growth of spheroids

Table 2 Concentration of major alloying elements in two steels used to demonstrate model, wt-%

Steel	C	Mn	Cr	Mo	Ni	Nb	V	Fe
10CrMoV	0·11	0·50	10·22	1·42	0·55	0·50	0·20	Bal.
2·25Cr1Mo	0·15	0·50	2·12	0·9	0·17	...	...	Bal.

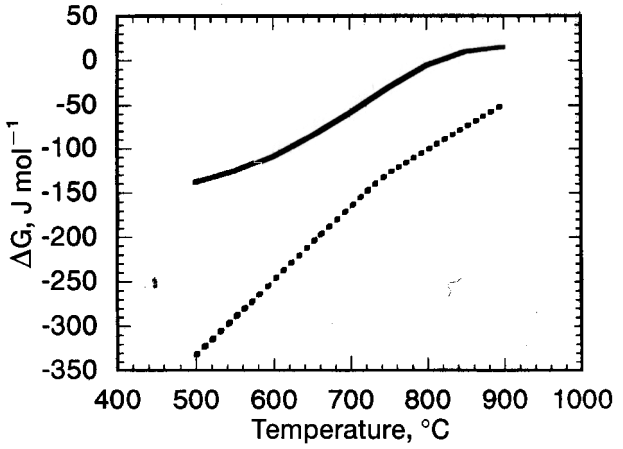

—— equilibrium; - - - - non-equilibrium

2 Calculated driving force ΔG for precipitation of M_2C carbides in 2·25Cr1Mo steel during elevated temperature tempering: in one case first phase to form is equilibrium cementite and in other case first phase to form is cementite with paraequilibrium composition; if equilibrium M_3C forms driving force for M_2C is considerably reduced

MODEL FOR M_2X PRECIPITATION

After M_3C has precipitated, M_2X is often the next precipitate to be observed,[18] but over a much larger time scale. Measurements of M_2X composition also show that this phase is closer to its equilibrium composition when it first forms.[16] The equilibrium composition of M_2X predicted using MTDATA is given for the two steels in Table 4.

Growth is known to be controlled by the diffusion of substitutional solute,[19] the particles growing in the form of needles. Zener's solution for the diffusion controlled growth of needles is known to be a good approximation for M_2X (Ref. 19)

$$g=\left(\frac{D\Omega}{4C_{14}r_c}\right);\quad \Omega=\left(\frac{\bar{c}-c^{\alpha\beta}}{c^{\beta\alpha}-c^{\alpha\beta}}\right) \qquad (23)$$

where Ω is the supersaturation, r_c is the critical radius of the tip of the needle at which the lengthening rate becomes zero, C_{14} is a constant ~ 1, $\bar{c}$ is the mean solute concentration, $c^{\alpha\beta}$ is the solute in the ferrite in equilibrium with M_2X, and $c^{\beta\alpha}$ is the solute in the M_2X in equilibrium with ferrite. Table 4 shows that 'M' in the M_2X consists largely of chromium. The diffusion coefficients for the substitutional species are all similar;[15] it was assumed, therefore, that diffusion of chromium to the needle tip was the rate controlling step in needle growth. Hence, the concentrations used are those for chromium. The critical radius is given by[3]

$$r_c=\frac{2c^{\alpha\beta}\Gamma}{(\bar{c}-2c^{\alpha\beta})};\quad \Gamma=\left(\frac{\sigma v^{\beta}}{kT}\right)\left(\frac{1-c^{\alpha\beta}}{c^{\beta\alpha}-c^{\alpha\beta}}\right) \qquad (24)$$

where Γ is the capillarity constant given by Ref. 3, k is the Boltzmann constant, v^{β} is the atomic volume, and σ is the surface energy of the M_2X. The values of v^{β} and σ were estimated as being $\sim 1{\cdot}9\times10^{-29}$ m^3 and 0·6 J m^{-2}, respectively. As shown by equation (23), the growth rate is time independent. The M_2X particles are modelled as cylinders growing at a constant rate with a constant aspect ratio. The volume of a needle which nucleated at a time τ at a later time t is, therefore, given by

$$V_{\beta}=\frac{\pi g(t-\tau)^3}{\phi^2} \qquad (25)$$

where ϕ is the needle aspect ratio: measurement showed this value to be ~ 15.

In independent work, the present authors have demonstrated that the kinetics of M_2X formation can not be adequately approximated by assuming that the needles simply grow from pre-existing nuclei, but that it is better to assume a constant nucleation rate. From classical theory, the nucleation rate per unit volume is given by

$$I=N\frac{kT}{h}\exp\left[\frac{-(G^*+Q^*)}{kT}\right] \qquad (26)$$

where h is the Planck constant, N is the number of nucleation sites per unit volume; Q^* is the energy required to transfer atoms across the α/β interface (assumed to be half the activation energy for volume diffusion),[3] and G^* is the free energy required to overcome the barrier to nucleation, given by

$$G^*=\frac{16\pi\eta^3\sigma^3}{3\Delta G_v^2} \qquad (27)$$

where σ is the surface energy per unit area, η is a shape factor, and ΔG_v is the chemical driving force for nucleation per unit volume of nucleus formed. The values N, σ, and η are unknown and difficult to determine experimentally. It was assumed that the nuclei are spherical, i.e. $\eta=1$. The values of N and σ were found by fitting the predicted results from the model to experimental data. It is likely that M_2X nucleates on certain preferred sites rather than nucleating homogeneously. These sites include dislocations and martensite lath boundaries. There is evidence in the literature that M_2X also forms by *in situ* transformation following nucleation at the M_3C/ferrite interface.[20] The equation describing the behaviour in this case is the same as equation (26) but the G^* term is different because the activation energy required for nucleation is much less than in the homogeneous case. This is equivalent to a reduction in the value of σ for heterogeneous nucleation. The value N is also different and will correspond to the number of heterogeneous nucleation sites. As both N and σ are found by fitting to experimental data, heterogeneous nucleation is implicitly accounted for.

The chemical driving force for the M_2X nucleation was derived from the driving force for transformation found using MTDATA. The transformation considered was

$$\alpha+M_3C_{para}\rightarrow\alpha+M_2X \qquad (28)$$

The left hand side is ferrite and M_3C with its paraequilibrium composition. The right hand side is the condition after complete transformation to M_2X which is ferrite (of a different composition) and M_2X with its equilibrium composition. The calculated driving forces for both steels over a range of temperatures are shown in Fig. 3*a*.

As time increases, the reaction shown by equation (28) will no longer represent the actual situation. For example, the M_3C will not remain at its paraequilibrium composition and, as it enriches, the driving force for M_2X precipitation

Table 3 Paraequilibrium and equilibrium concentrations of principal species in M_3C for 10CrMoV steel heat treated at 500°C, at.-%

	Fe	C	Cr	Mo
Paraequilibrium	65·0	25	8·2	0·62
Equilibrium	4·3	25	69·8	0·03

Table 4 Equilibrium concentrations of principal species in M_2X at 500°C, at.-%

Steel	C	Cr	Mo	N	V
10CrMoV	23·2	47·1	12·7	10·1	6·4
2·25Cr1Mo	33·3	40·4	24·4		

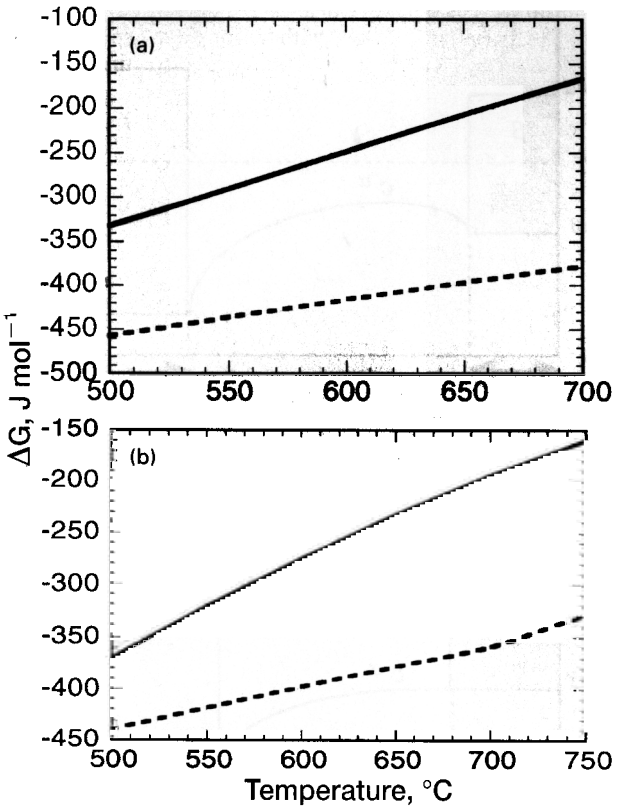

—— 2·25Cr1Mo; ---- 10CrMoV
a M_2X; *b* $M_{23}C_6$

3 Driving force ΔG for given phase precipitation in system containing ferrite and cementite with paraequilibrium composition for 10CrMoV steel and 2·25Cr1Mo steel

will decrease. These effects are accounted for by suitable modification of the driving force and this is discussed in the 'Solute partitioning effects' section below.

MODEL FOR $M_{23}C_6$ PRECIPITATION

The carbide $M_{23}C_6$ is frequently found in a wide range of power plant steels, and in the 10CrMoV alloys is the most stable carbide which rapidly dominates the microstructure even after just 4 h at 600°C. In 2·25Cr steels, on the other hand, $M_{23}C_6$ precipitation takes considerably longer (~1000 h at 600°C).[18] Experimental evidence shows that $M_{23}C_6$ is close to its equilibrium composition when it starts to form.[21] Equilibrium compositions as calculated by MTDATA are given in Table 5.

It can be seen that $M_{23}C_6$ is predominantly a chromium carbide. It is reasonable, therefore, to assume that it grows at a rate controlled by the diffusion of chromium through the ferrite. As the particles grow approximately isotropically, they are represented as spheres, the radius of each of which is given by

$$r = \chi(t-\tau)^{1/2} \quad \ldots\ldots\ldots\ldots\ldots\ldots \quad (29)$$

where χ is the three-dimensional parabolic rate constant. The Zener approximation for low supersaturations was used to give an expression for χ in terms of the compositions

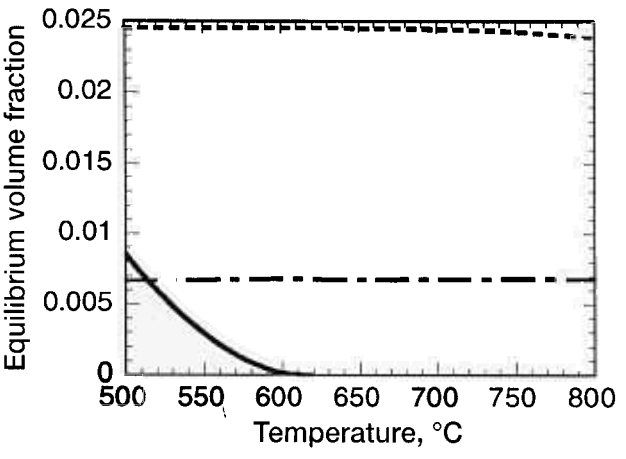

---- $M_{23}C_6$; —— Laves; —·— M_2X

4 Volume fraction of phases in thermodynamic equilibrium as function of temperature (calculated using MTDATA) for 10CrMoV steel

of ferrite and $M_{23}C_6$ (β) which were calculated using MTDATA. A typical value for chromium supersaturation in the $M_{23}C_6$–ferrite system is 0·02 (2·25Cr1Mo steel at 500°C), which is sufficiently small for the following approximation to be valid

$$\chi \simeq D^{1/2}2^{1/2}\frac{(\bar{c}-c^{\alpha\beta})^{1/2}}{(c^{\beta\alpha}-\bar{c})^{1/2}} \quad \ldots\ldots\ldots\ldots \quad (30)$$

The volume of an individual particle at a time $t-\tau$ is given by

$$V = (4/3)\pi\chi^3(t-\tau)^{3/2} \quad \ldots\ldots\ldots\ldots \quad (31)$$

The nucleation behaviour of $M_{23}C_6$ was modelled in much the same way as that of M_2X. The appropriate chemical driving force is now given by consideration of the reaction

$$\alpha + M_3C_{para} \rightarrow \alpha + M_{23}C_6$$

As in the case of M_2X nucleation, this driving force will be modified as time increases and other intermediate transformations (e.g. M_2X precipitation) occur. The way the driving force is modified to account for this is discussed in the 'Solute partitioning effects' section below. Figure 3*b* shows how the driving force for $M_{23}C_6$ precipitation varies with temperature for the 10CrMoV steel and the 2·25Cr1Mo steel.

The number of sites and surface energy for nucleation were found, as in the M_2X case, by fitting the predicted results to experimental data. As before, this will account for the fact that the nucleation of $M_{23}C_6$ occurs largely on preferred sites rather than homogeneously.

MODEL FOR LAVES PHASE PRECIPITATION

Laves phase is an intermetallic compound with the general composition Fe_2M. The 'M' can be tungsten, molybdenum, or some combination of both. It is often observed in the 9–12 wt-%Cr steels containing tungsten and molybdenum after long term exposure to elevated temperatures where it is an equilibrium phase.[22] Typically, there is a temperature above which Laves phase is no longer a stable phase. In the case of the 10CrMoV steel under present investigation, this temperature is relatively low as shown in Fig. 4, which

Table 5 Equilibrium concentrations of principal species in $M_{23}C_6$ at 500°C, at.-%

	Fe	C	Cr	Mo
10CrMoV	6·2	20·7	62·6	10·3
2·25Cr1Mo	21·0	20·7	48·0	10·3

Table 6 Equilibrium concentrations of principal species in Laves phase for 10CrMoV type steel, at.-%

	Fe	Cr	Mo	
500	60·7	6·0	31·3	2·0
550	62·6	4·0	30·0	3·4

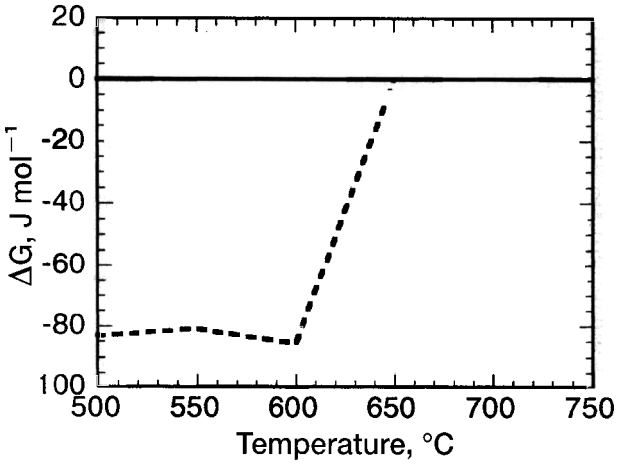

—— 2·25Cr1Mo; - - - - 10CrMoV

5 Driving force ΔG for Laves phase precipitation in system containing ferrite and cementite with paraequilibrium composition for 10CrMoV steel and 2·25Cr1Mo steel

is a plot of the volume fraction of the equilibrium phases as a function of temperature. The calculated equilibrium composition of Laves phase in the 10CrMoV steel is given for two temperatures in Table 6.

It can be seen that, in this steel, Laves phase is molybdenum rich. It was assumed, therefore, that Laves phase grows at a rate controlled by the diffusion of molybdenum. The particles were assumed to grow isotropically and were represented as spheres as in the case of $M_{23}C_6$ precipitation. The same model was used as for $M_{23}C_6$ with the appropriate molybdenum concentrations being substituted into the growth equations. The nucleation behaviour was also modelled in an identical manner to the other phases, with the appropriate chemical driving force being given by consideration of the reaction

$$\alpha + M_3C_{para} \rightarrow \alpha + \text{Laves}$$

This gives the maximum conceivable value for the driving force. Figure 5 shows how this driving force varies with temperature for the 10CrMoV steel and the 2·25Cr1Mo steel. It is apparent that there is only a driving force for Laves phase precipitation in the 10CrMoV steel. Clearly, in reality, this driving force will be considerably reduced by the precipitation of intermediate phases, as discussed in the section on 'Solute partitioning effects' below. The number of sites and surface energy were found by comparing the predicted and experimental results, although the lack of suitable experimental results means that these parameters are probably not fully optimised.

CALCULATING PHASE COMPOSITIONS

The growth rates of all the phases being modelled depend on the concentrations of the alloying elements at the interface in both the parent and product phases. For all the phases except cementite, precipitation occurs by diffusion of both substitutional and interstitial atoms, and it is expected, therefore, that the composition each phase adopts will be such that the Gibbs free energy of the system is minimised. The program MTDATA was used to calculate each phase using this criterion. The procedure used has two stages. The first is the calculation of the final equilibrium state, allowing all the phases included in the model to be potential equilibrium phases. This calculation gives the composition of the equilibrium precipitates and the associated ferrite. By suppressing the equilibrium precipitate phases and recalculating, the next most stable phases and associated compositions are found. This

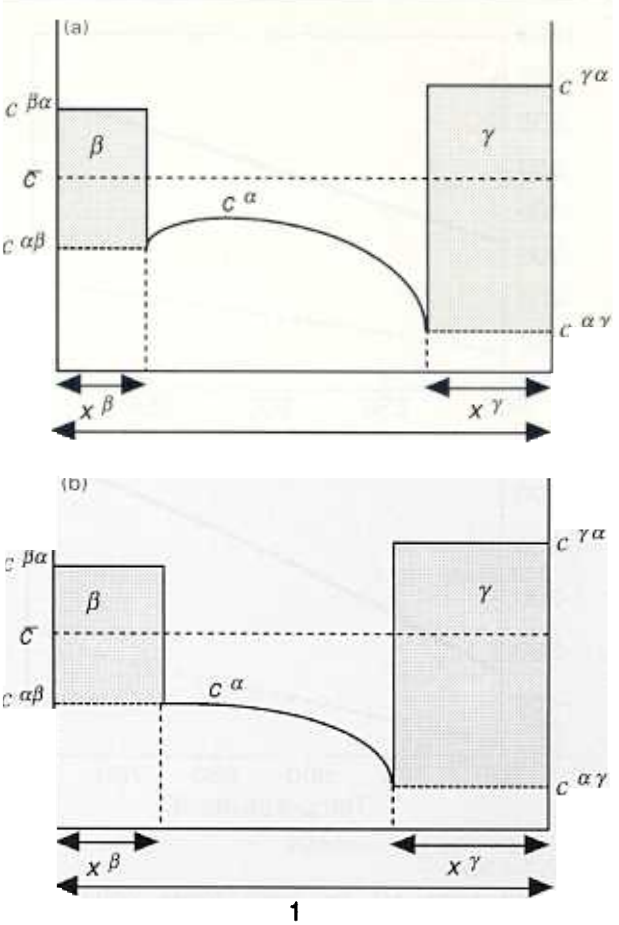

a both β and γ precipitating; *b* precipitation of β has been completed

6 Distribution of solute at given stages

procedure was repeated for all the phases where the composition results from minimisation of the Gibbs free energy (i.e. M_2X, $M_{23}C_6$, and Laves phase). For example, the composition of the M_2X in the 2·25Cr1Mo steel given in Table 4 was calculated by first suppressing $M_{23}C_6$, which is the more stable phase, and then calculating the new equilibrium state.

Solute partitioning effects

It is not possible to rigorously account for soft impingement in a method based on the extended volume concept, and for a problem as complex as power plant steels. However, the observed effects undoubtedly can not be simulated without soft impingement. A common approximation in these circumstances is to take account of the average solute concentration change caused by precipitation; this is explained below.

Each precipitating phase will consume or reject atomic species into the untransformed matrix, whose subsequent transformation behaviour, therefore, will be altered. Consider the precipitation of β and γ from α, which initially has a uniform composition. Figure 6 shows how the distribution of solute might change during precipitation at an intermediate stage when both β and γ are precipitating (Fig. 6*a*), and at a later time when the formation of β is just complete (Fig. 6*b*).

For the situation illustrated, the maximum fraction of each phase is designated x_M and the fraction at any instant x. The maximum fraction is given by a lever rule

$$x_M^{\beta} = \frac{\bar{c} - c^{\alpha\beta}}{c^{\beta\alpha} - c^{\alpha\beta}} \quad (32)$$

It is then possible to define a parameter Φ for each phase, such that $\Phi = x/x_M$, which changes from 0 to 1 during the course of the transformation. When there is more than one precipitating phase, Φ can be generalised to account for concentration changes caused by each new phase. Identifying each of the n precipitating phases by a subscript $i = 1, ..., n$ gives

$$\Phi_i = \frac{\sum_{i=1}^{n} (x_i)(c^{i\alpha} - c^{\alpha i})}{(\bar{c} - c^{\alpha i})} \quad \ldots\ldots\ldots\ldots (33)$$

The approximation is now made that the chemical driving force ΔG for the formation of each phase is related linearly to Φ_i

$$\Delta G_i\{\Phi\} = (1 - \Phi)\Delta G_i\{\Phi = 0\} \quad \ldots\ldots\ldots (34)$$

where the braces are used to identify that ΔG is a function of Φ.

The definition of Φ is a little different for cementite, which in the present context precipitates rapidly by paraequilibrium transformation. The parameter Φ is defined, therefore, to reflect its subsequent change in composition by the diffusion of solute into the cementite

$$\Phi_{M_3C} = \frac{c - \bar{c}'}{c^{M_3C\alpha} - \bar{c}'} \quad \ldots\ldots\ldots\ldots (35)$$

where $\bar{c}'$ is the mean solute level in the matrix at any instant, and a function of all the other phases

$$\bar{c}' = \frac{\bar{c} - \sum_{i \neq 1}^{n} x_i c^{i\alpha}}{1 - \sum_{i=1}^{n} x_i} \quad \ldots\ldots\ldots\ldots (36)$$

The analysis in terms of Φ is a crude approximation to what is commonly referred to as soft impingement phenomena.[3] The concentration gradients in the ferrite for the precipitation reactions that occur in power plant steels are very shallow, so the approximation may be justified.

As many of the phases in the precipitation sequence are metastable, they must tend to dissolve as soon as the concentration in the ferrite falls below that consistent with metastable equilibrium with the precipitate (i.e. $\bar{c}' \leqslant c^{\alpha i}$). This is discussed further in the 'Dissolution of phases' section below.

Computation of overall transformation kinetics

Having incorporated all the nucleation and growth phenomena into a computer program, it becomes possible to solve for simultaneous transformation kinetics. The following explanation is, for the sake of simplicity, based on three precipitation reactions, although the method can be made much more general. The three precipitates are designated θ, β, and γ, to represent M_3C, M_2X, and $M_{23}C_6$, respectively.

An iterative procedure is used, as described in the 'Complex simultaneous reactions' section above:

(i) the time t and volume fractions of β and γ are set initially to zero. The concentration of substitutional solute in the cementite θ is set to mean solute composition, consistent with its paraequilibrium growth mechanism

(ii) the growth and nucleation rates for β and γ are calculated using the current value for the solute concentration in the matrix

(iii) the time t is incremented by a small step Δt. The additional volume of each phase precipitated in the interval $t \rightarrow t + \Delta t$ is calculated while at the same time allowing cementite to change its chemical composition (i.e. tend towards equilibrium)

(iv) the volumes of β and γ are updated, as is the composition of the cementite

(v) the amount of solute removed from ferrite due to the precipitation of β and γ, and due to the change in cementite composition, is calculated, and the mean ferrite composition modified accordingly. All the driving force terms and nucleation and growth rate terms are modified to be consistent with the change in ferrite chemical composition

(vi) steps (ii)–(v) are repeated until $t = t_f$, where t_f is the time of heat treatment at the temperature concerned

(vii) the volume fractions of β and γ at time t_f are, thus, output along with the composition of θ.

VOLUME INCREMENT β AND γ

A detailed description of the method used for spherical precipitates (e.g. $M_{23}C_6$) is now given, and its adaptation for other shapes.

During diffusion controlled growth of spherical particles, each dimension of the growing particle increases in proportion to the square root of the time (equation (29)). Considering small increments in time, each of magnitude Δt, it follows that the corresponding change in the extended volume of spherical particles beginning with the first increment of time is given by

$$\Delta V_1^e = (I_1 V \Delta t_1)(C\chi_1^3 \Delta t_1^{3/2}) \quad \ldots\ldots\ldots (37)$$

where $C = 4\pi/3$ and the numerical subscripts identify the sequence of time increments. The two terms on the right represent the number of particles nucleated and the contribution of each particle to the extended volume, respectively.

The change in extended volume for the second interval Δt_2 is then

$$\Delta V_2^e = (I_2 V \Delta t_2)(C\chi_2^3 \Delta t_2^{3/2}) + \tfrac{3}{2} I_1 V \Delta t_1 C\chi_2^3 (\Delta t_1 + \Delta t_2)^{1/2} \Delta t_2 \quad \ldots\ldots\ldots (38)$$

where the second term on the right is the contribution resulting from the increase in the size of particles which were nucleated in the first time interval. Since the time intervals are of equal size, this equation can be written

$$\Delta V_2^e = CV\Delta t^{5/2} \chi_2^3 (I_2 + \tfrac{3}{2}(2)^{1/2} I_2) \quad \ldots\ldots\ldots (39)$$

or, in general, for the mth time increment, the corresponding change in extended volume is given by

$$\Delta V_m^e = CV\Delta t^{5/2} \chi_m^3 (I_m + \tfrac{3}{2}\sqrt{2} I_{m-1} \ldots + \tfrac{3}{2}\sqrt{m} I_1) \quad (40)$$

For each interval, the increase in extended volume for a specific phase γ is converted to a corresponding change in actual volume of γ as before, allowing now for the coexistence of n phases

$$\Delta V_\gamma = \left(1 - \frac{\sum_{i=1}^{n} V_i}{V}\right) \Delta V_\gamma^e \quad \ldots\ldots\ldots (41)$$

where V_i is the actual volume of the ith phase. The total volume of γ, thus, is updated

$$V_\gamma^{new} = V_\gamma^{old} + \Delta V_\gamma \quad \ldots\ldots\ldots (42)$$

This procedure is repeated for all the intervals from $t = 0 \rightarrow t_f$, at which time the final volume is output along with the time. The same approach is used for all phases with a spherical morphology (Laves phase and $M_{23}C_6$ in this case). For needle shaped particles, the basic method is the same but the expression for the extended volume is different. Equation (25) gives the volume of a single needle shaped particle of β at a time $(t - \tau)$ after its nucleation. This may also be written as $V_\beta = C_\beta [g(t - \tau)]^3$ where $C_\beta = \pi/\phi^2$. It

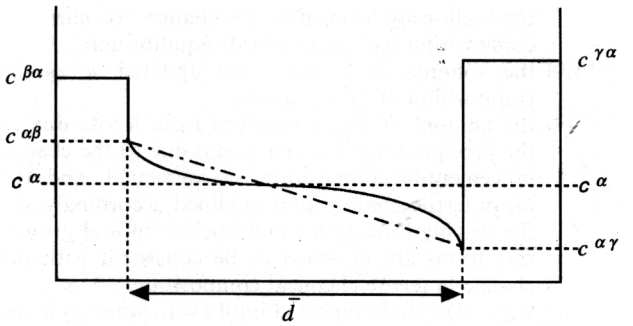

7 Schematic illustration of composition profile when β is dissolving and γ is precipitating: chain dotted line shows mean concentration gradient from β to γ

follows that

$$\Delta V_m^e = C_\beta V \Delta t_m^4 g_m^3 [I_m + 3(2)^2 I_{m-1} \quad 3(m+1)^2 I_1] \quad \ldots\ldots\ldots\ldots (43)$$

This approach can be used for any number of phases at the risk of increasing the computational time and memory requirements. One thousand time increments were used for each temperature after checking that decreasing the increment did not make any significant difference to the results.

Dissolution of phases

Metastable phases must eventually dissolve as equilibrium is approached. Figure 7 illustrates the circumstances in which metastable β begins to dissolve when the concentration in the matrix away from the β particle drops below $c^{\alpha\beta}$, with a tendency for solute to be released from the dissolving β to the more stable γ.

During diffusion controlled dissolution of a particle of radius r, a consideration of mass balance at the β/α interface requires that

$$\frac{dr}{dt}(c^{\beta\alpha} - c^{\alpha\beta}) = -D_\alpha \frac{dc}{dr} \quad \ldots\ldots\ldots\ldots (44)$$

The term on the left hand side is the rate at which solute is released into the matrix as the particle dissolves, which must be carried away by diffusion as represented by the right hand side of the equation. If the concentration gradient is assumed to be constant (the Zener linearised gradient approximation) then

$$\frac{dc}{dr} = -\frac{(c^{\alpha\gamma} - c^{\alpha\beta})}{\bar{d}} \quad \ldots\ldots\ldots\ldots (45)$$

where $\bar{d}$ is the mean diffusion distance between the β and γ particles, given by

$$\bar{d} = (P_\beta + P_\gamma)^{-1/3} \quad \ldots\ldots\ldots\ldots (46)$$

where P is a number density of particles, assumed constant throughout dissolution; smaller particles should, in reality, vanish before larger ones but, for simplicity, it is assumed that the whole process can be represented by a mean particle size of radius $\bar{r}$. With this approximation, it follows that

$$\frac{dV_\beta}{dt} = 4\pi \bar{r}^2 \frac{D_\alpha}{\bar{d}} \frac{(c^{\alpha\beta} - c^{\alpha\gamma})}{(c^{\beta\alpha} - c^{\alpha\beta})} \quad \ldots\ldots\ldots\ldots (47)$$

In the case of a needle shaped particle dissolving (e.g. M_2X), the reduction in volume is given by

$$\frac{dV_\beta}{dt} = -\frac{3\pi l^3 (c^{\alpha\beta} - c^{\alpha\gamma})}{\phi \bar{d}(c^{\beta\alpha} - c^{\alpha\beta})} \quad (48)$$

where $c^{\beta\alpha}$ and $c^{\alpha\beta}$ now refer to the concentrations of solute in the needle shaped phase, and l is the needle length which decreases as the particles dissolve.

There is a slight difference when considering the dissolution of M_3C since its composition varies with time. Enrichment will stop, and dissolution will start when the extent of reaction Φ for M_3C equals 1. Dissolution may then be dealt with in the same way as for other phases, with the solute concentration in the M_3C fixed from the point when enrichment stopped.

Conclusions

The classical Johnson–Mehl–Avrami theory describing the rate at which a phase precipitates during solid state transformation has been adapted to deal with the simultaneous precipitation of many phases. In the simplest of cases, where the fractions of the product phases are related by constants, it has been possible to solve the problem rigorously. An approximate method has been necessary to deal with cases where the composition of the matrix changes during the course of the transformations. The method, in principle, enables any number of simultaneous precipitation reactions to be modelled theoretically, relying only on the availability of interfacial energies, number densities of nucleation sites, and thermodynamic data. It is possible, therefore, to attempt a prediction of the time–temperature–transformation diagram for tempering reactions in secondary hardening steels as a function of the chemical composition and heat treatment. Such calculations are presented in Part 2 (Ref. 23).

Acknowledgements

The authors are grateful to National Power plc for financial support via Dr David Gooch. They would also like to thank David Gooch, Andrew Strang, Rod Vanstone, and Rachel Thomson for their help during the course of some of this work. The help of Hugh Davies and Susan Hodgson with the provision and support of MTDATA is greatly appreciated. One of the authors (HKDHB) is grateful to the Royal Society for a Leverhulme Trust Senior Research Fellowship.

References

1. K. J. IRVINE: in 'Materials in power plant', 1–10; 1975, London, The Institution of Metallurgists.
2. I. M. AUSTIN, P. McINTYRE, and E. F. WALKER: in 'Materials in power plant', 120–127; 1975, London, The Institution of Metallurgists.
3. J. W. CHRISTIAN: 'Theory of transformations in metals and alloys', 2nd edn, Part I; 1975, Oxford, Pergamon Press.
4. M. UMEMOTO, A. HIRAMATSU, A. MORIYA, T. WATANABE, S. NANBA, N. NAKAJIMA, G. ANAN, and Y. HIGO: *ISIJ Int.*, 1992, **32**, 306–315.
5. H. K. D. H. BHADESHIA, L.-E. SVENSSON, and B. GRETOFT: *Acta Metall.*, 1985, **33**, 1271–1283.
6. E. ANELLI, S. AMATO, and P. E. DINUNZIO: 'Mathematical model for transformation from deformed austenite', European Coal and Steel Community, Report 7769R', Centro Sviluppo Materiali, Rome, Italy, 1992.
7. H. K. D. H. BHADESHIA: 'Mathematical modelling of weld phenomena 2', (ed. H. Cerjak), 71–118; 1995, London, The Institute of Materials.
8. H. K. D. H. BHADESHIA: *Mater. Sci. Technol.*, 1989, **5**, 131–137.
9. S. V. TSIVINSKY, L. I. KOGAN, and R. I. ENTIN: in 'Problems of metallography and the physics of metals', (ed. B. Ya. Lybubov), 1985–1991; 1955, Moscow, State Scientific Press (translation, 1959, New York, Consultants Bureau).

10. J. CHANCE and N. RIDLEY: *Metall. Trans. A*, 1981, **21A**, 1205–1213.
11. A. HULTGREN: *Jernkontorets Ann.*, 1951, **135**, 403.
12. M. HILLERT: *Jernkontorets Ann.*, 1952, **136**, 25–37.
13. E. RUDBERG: *Jernkontorets Ann.*, 1952, **136**, 91.
14. 'MTDATA: Metallurgical and thermochemical databank', National Physical Laboratory, Teddington, Middx, UK, 1995.
15. J. FRIDBERG, L.-E. TORNDAHL, and M. HILLERT: *Jerkontorets Ann.*, 1969, **153**, 263–276.
16. R. C. THOMSON: PhD thesis, University of Cambridge, 1992.
17. M. F. ASHBY and D. R. H. JONES: 'Engineering materials 2', 315; 1992, Oxford, Pergamon Press.
18. R. G. BAKER and J. NUTTING: *J. Iron Steel Inst.*, 1959, **192**, 257–268.
19. M. G. HALL, K. R. KINSMAN, and H. I. AARONSON: *Metall. Trans.*, 1972, **3**, 1320–1322.
20. D. RAYNOR, J. A. WHITEMAN, and R. W. K. HONEYCOMBE: *J. Iron Steel Inst.*, 1966, **204**, 349–354.
21. R. C. THOMSON and H. K. D. H. BHADESHIA: *Metall. Trans. A*, 1992, **23A**, 1171–1179.
22. H. MIMURA, M. OGHAMI, H. NAOI, T. FUJITA, J. HALD and R. BLUM: *Zairyo to Purosescu (CAMP–ISIJ)*, 1994, **7**, 809.
23. J. D. ROBSON and H. K. D. H. BHADESHIA: *Mater. Sci. Technol.*, 1997, **13**, 640–645.